

HOKKAIDO UNIVERSITY

Title	Development and perfomance of a miniaturised spin rotator suitable for neutron interferometer experiments
Author(s)	Danner, Armin; Demirel, Buelent; Sponar, Stephan et al.
Citation	Journal of Physics Communications, 3(3), 035001 https://doi.org/10.1088/2399-6528/ab0805
Issue Date	2019-03
Doc URL	https://hdl.handle.net/2115/74029
Rights(URL)	https://creativecommons.org/licenses/by/3.0/
Type	journal article
File Information	Danner_2019_J._Phys._Commun._3_035001.pdf



Hokkaido University Collection of Scholarly and Academic Papers : HUSCAP

Journal of Physics Communications

PAPER • **OPEN ACCESS**

Development and perfomance of a miniaturised spin rotator suitable for neutron interferometer experiments

To cite this article: Armin Danner *et al* 2019 *J. Phys. Commun.* **3** 035001

View the article online for updates and enhancements.

This content was downloaded from IP address 133.87.166.83 on 15/05/2019 at 08:29

Journal of Physics Communications



OPEN ACCESS

RECEIVED
17 January 2019

REVISED
31 January 2019

ACCEPTED FOR PUBLICATION
18 February 2019

PUBLISHED
6 March 2019

Original content from this work may be used under the terms of the Creative Commons Attribution 3.0 licence.

Any further distribution of this work must maintain attribution to the author(s) and the title of the work, journal citation and DOI.



PAPER

Development and perfomance of a miniaturised spin rotator suitable for neutron interferometer experiments

Armin Danner[1], **Bülent Demirel**[1], **Stephan Sponar**[1] and **Yuji Hasegawa**[1,2]

[1] Atominstitut, TU Wien, Stadionallee 2, 1020 Vienna, Austria
[2] Department of Applied Physics, Hokkaido University, Kita-ku, Sapporo 060-8628, Japan

E-mail: armin.danner@tuwien.ac.at and yuji.hasegawa@tuwien.ac.at

Keywords: quantum physics, neutron optics, spin-rotation coupling

Abstract

A miniaturised versatile spin rotator for application in neutron interferometer experiments is developed. The coil design without material in the beam path allows for a magnetic field adjustable to an arbitrary direction perpendicular to the neutron beam. The field simulations show a homogeneous field over the beam cross-section of 8 mm $\times$ 5 mm and a field transition $\lesssim$20 mm from inside to outside. The performance of the fabricated miniaturised coil was quantified by carrying out the polarimeter experiment of Demirel *et al* (*New J. Phys.*, **17**:023065, 2015) regarding spin-rotation coupling. The high efficiency spin manipulations by the implemented rotating magnetic field results in a linear dependence between the phase shift and the rotation frequency. In near future, the spin rotator will be used to investigate spin-rotation coupling in a related interferometer experiment.

1. Introduction

All experiments on earth are carried out in a rotating frame of reference. Consequently, rotating systems have been investigated both theoretically and experimentally for the last century. The coupling between a rotation vector $\vec{\Omega}$ and the orbital angular momentum $\vec{L}$ is described by an additional interaction term $\sim\vec{\Omega}\cdot\vec{L}$ in the Hamiltonian referred to as the Sagnac effect [1]. Generalising the coupling from the orbital angular momentum to the total angular momentum $\vec{J}=\vec{L}+\vec{S}$ adds the Hamiltonian $\hat{H}_{\mathrm{SR}}$ of the spin-rotation coupling [2]

$$\hat{H}_{\mathrm{SR}}\sim\vec{\Omega}\cdot\vec{S}. \tag{1}$$

In a series of articles [3, 4], Mashhoon *et al* proposed to measure the coupling of single neutrons in a neutron interferometer experiment. By modifying the latest proposal [4] to a neutron polarimeter experiment, Demirel *et al* [5] investigated the spin-rotation coupling using the set-up of a Ramsey interferometer [6] and a rotating magnetic field as rotating system. The relative phase between both spin eigenstates of the rotation was linearly dependent on the rotation frequency in accordance with (1). The central spin manipulating coil, henceforth called the *rotating field generator* (RFG), used by Demirel *et al* was 200 mm long and had material in the neutron beam. The paper was critised because the spin evolutions can also be described by the semi-classical Bloch equation (see (4)). To overcome this critisism, the concept of the latest proposal by Mashhoon and Kaiser [4] of an interferometer experiment is modified to the situation depicted in figure 1 and an induced phase proportional to the rotation frequency cannot be classically described in this set-up. For this purpose, the rotating field generator is further developed. In this paper, we present the results of this process.

In neutron optics, coils are often used to induce an interaction between their magnetic fields and the spin of neutrons $S=1/2\,\hbar$ which composes a two-level system. While neutron polarimetry [7–10] allows the observation of the relative phase between interfering spin states, neutron interferometry [11–16] enables the observation of relative phases in a multi-level system of different path states. The field of a coil is desirably homogeneous over the beam cross-section to produce similar spin manipulations to all neutrons or wave packets regardless of their passage through the field. Sudden magnetic field transitions are indispensable for deterministic spin evolutions and are usually guaranteed by coils with wires in the beam (e.g. [10]). The field

© 2019 The Author(s). Published by IOP Publishing Ltd

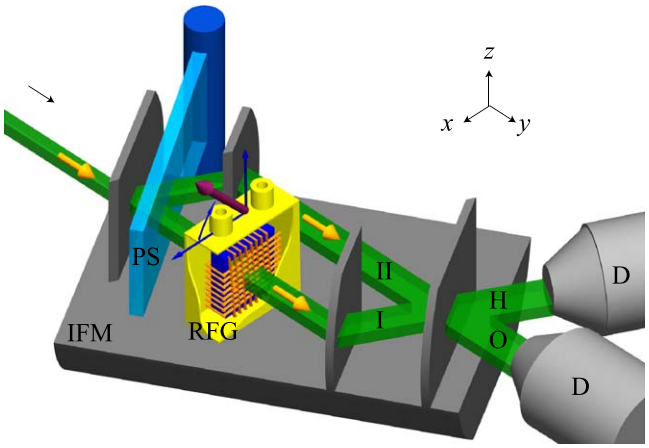


Figure 1. Concept of an interferometer experiment testing for spin-rotation coupling. A monochromatic beam of forward polarised neutrons (orange arrows) is split into two arms at the first plate of the interferometer (IFM). A phase shifter (PS) induces a relative phase between the arms which interfere behind the last plate as O and H-beams (O and H). Detectors (D) measure the intensities. The rotating field generator (RFG) inside a water cooled housing generates a field (purple arrow) $\vec{B} = B_0(\cos(\Omega t),\ 0,\ \sin(\Omega t))^T$ inducing a cyclic spin rotation in path I while the spin orientation is static in path II. When recombined at the last plate, the spins of both paths are aligned parallel. A phase induced between them changes the intensities in both detectors.

orientation within such coils is perpendicular to the direction of the neutron beam and very homogeneous while their outer flux is negligible. Such coil designs could also be useful for spin manipulations on single paths of a neutron interferometer. However, the homogeneity of the field is achieved with coil diameters too large to fit into a relatively small interferometer crystal composed of silicon. Moreover, the sudden field transition is achieved with material in the beam, i.e. wires which are inevitably inhomogeneously deployed over the beam cross-section. Thus, the phase relation to another arm of an interferometer strongly depends on the position in the beam cross-section and the contrast

$$C = \frac{I_{\max} - I_{\min}}{I_{\max} + I_{\min}}, \tag{2}$$

of interferograms with maximum and minimum intensity, is consequently reduced.

Another type of coils used in neutron optics are RF spin flippers [17–21]. They generate an oscillating field in beam direction with frequencies ~50kHz with a solenoid around the axis of the beam. In particle physics, coils are used for precise manipulations of trajectories of charged particles with superconductors, such as in particle accelerators [22] or in hadron cancer therapy [23].

The structure of our paper is as follows: in section 2, the theory regarding spin rotation coupling and the concept of the polarimeter experiment are presented briefly. While the development process is described in section 3, in section 4 the experimental performance tests are described which are a repetition of the experiment of Demirel *et al* [5].

2. Theory regarding spin-rotation coupling

The polarisation vector $\vec{P}$ is given by the expectation value of the spin operator $\vec{\sigma}$ formulated as

$$\vec{P}(t) = \langle \chi(t)|\ \vec{\sigma}\ |\chi(t)\rangle \tag{3}$$

where χ denotes the spinor part of the wave function. In a magnetic field $\vec{B}$, the time derivative of the polarisation vector is described by the Bloch equation which is written as

$$\frac{\mathrm{d}\vec{P}}{\mathrm{d}t}(t) = \frac{2|\vec{\mu}|}{\hbar}\vec{P}(t) \times \vec{B}(t) \tag{4}$$

with the magnetic moment of the neutron $\vec{\mu}$. While the orientation of the polarisation vector is described by this equation, additional dynamical and geometrical phases of spin states [24–30] are described by the Schrödinger equation.

During the following calculus, only the features of the spin-rotation coupling essential for the design and the experimental test of the presented coil are highlighted. More detailed accounts are found in references [31–33]. For technical reasons, with the neutrons propagating in y-direction, a rotating magnetic field with the field amplitude B_0 and the angular velocity Ω is most easily implemented as rotating around the beam direction in the

$x-z$-plane which is written as

$$\vec{B}(t) = B_0(\cos(\Omega t),\ 0,\ \sin(\Omega t))^T. \tag{5}$$

The system of a neutron in a magnetic field is described by the Hamiltonian

$$\hat{H} = -\frac{\hbar^2}{2m}\nabla_y^2 - \vec{\mu}\cdot\vec{B} \tag{6}$$

with the neutron's mass m and its magnetic moment $\vec{\mu}$. The solution of the Pauli-Schrödinger equation is then written as [33]

$$\psi(y,\ t) = \frac{1}{\sqrt{2\pi}}\exp\left[\mathrm{i}(ky-\omega t)\right]\exp\left(\mathrm{i}\frac{\Omega t}{2}\hat{\sigma}_y\right)\exp\left(-\mathrm{i}\frac{\vec{\alpha}\cdot\vec{\sigma}}{2}\right)\xi_{\mathrm{rot}}(0) \tag{7}$$

with the wave number k, the angular velocity $\omega = E_{\mathrm{kin}}/\hbar$ dependent on the kinetic energy E_{kin}, the vector $\vec{\sigma}$ composed of the Pauli matrices, an initial spin state $\xi_{\mathrm{rot}}(0)$ in the frame of reference rotating with the magnetic field, the vector representing the rotation axis in the co-rotating frame of reference

$$\vec{\alpha} = \alpha\hat{\alpha} = (\omega_0 t,\ \Omega t,\ 0)^T, \tag{8}$$

and the Larmor precession angular velocity

$$\omega_0 = -2\mu B_0/\hbar. \tag{9}$$

In (7), two exponentials, with a product of the angular velocity Ω and Pauli matrices in their arguments, can be identified as spin-rotation couplings as in (1).

In the proposals for interferometric experiments by Mashhoon *et al* [3, 4], they assume a π-flip of the spin orientation in both arms of an interferometer. In one arm, this is achieved with a static magnetic field while in the other arm the field is rotating. Because the field is time-dependent, in general the kinetic energy of the neutron is changed and the predicted intensities in the H and O-beams oscillate with the angular velocity Ω of the rotating magnetic field. This proposed procedure makes time-dependent measurements necessary. In a polarimeter experiment, Demirel *et al* implemented cyclic spin evolutions on the Bloch sphere which make the output of the spin manipulation static. A simple condition for cylic spin evolutions for an initial state $|\pm y\rangle$ is given by

$$\pm\mathbb{1} = \exp(-\mathrm{i}\frac{\vec{\alpha}\cdot\vec{\sigma}}{2}) \equiv \mathbb{1}\cos\frac{\alpha}{2} - \mathrm{i}\hat{\alpha}\cdot\vec{\sigma}\sin\frac{\alpha}{2} \Rightarrow \alpha = 2\pi n, \tag{10}$$

with an integer n. A fixed value of n implies a lower field amplitude for higher rotation frequencies $f = \Omega/2\pi$ via the relation

$$B_0(\Omega) = \frac{\hbar}{2|\vec{\mu}|}\left[\left(\frac{2\pi n}{T}\right)^2 - \Omega^2\right]^{1/2} \tag{11}$$

and, with an additionally fixed interaction time T, a maximum frequency $f_{\mathrm{max}} = n/T$ for cyclic evolutions. The time evolutions carried out in the experiment with $n = 1$ in (10) are presented in figure 2. The induced phases can be interpreted as a combination of dynamical and geometric phases whereupon the latter are associated with the solid angles enclosed by the evolution paths.

After the interaction time T and for an initial spin state $|\pm y\rangle$, variations of the rotation frequency will then only change the henceforth called *Mashhoon phase* ϕ_{Mh} which is given by the argument of the second exponential in (7) as

$$\phi_{\mathrm{Mh}} = \frac{\Omega T}{2}\hat{\sigma}_y. \tag{12}$$

In this case, the states $|\pm y\rangle$ are eigenstates of the spin manipulation. As a result, an initial spin state $|+z\rangle$ in the laboratory frame of reference yields a final spin state

$$|\xi(\Omega,\ T)\rangle = \frac{1}{\sqrt{2}}\left(\exp\left(\mathrm{i}\frac{\Omega T}{2}\right)|+y\rangle - \exp\left(-\mathrm{i}\frac{\Omega T}{2}\right)|-y\rangle\right). \tag{13}$$

Thereby, the inital polarisation vector in z-direction is rotated around the y-axis dependent on the rotation frequency written as

$$\vec{P}(\Omega,\ T) = (\sin(\Omega T),\ 0,\ \cos(\Omega T))^T. \tag{14}$$

In a neutron polarimeter, this allows an indirect observation of the phase shift due to spin-rotation coupling which is the concept of the experiment in section 4.3.

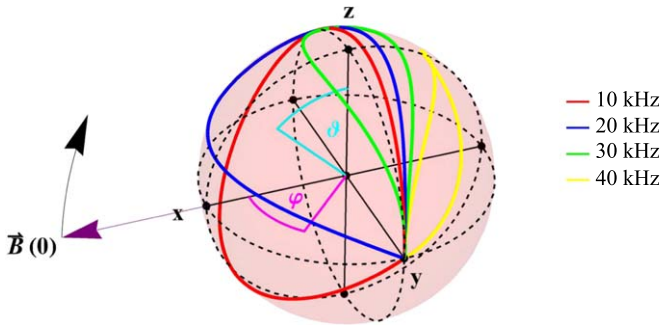


Figure 2. The unit sphere with the coordinates of the polar angle ϑ and the azimuthal angle φ of polarisation vectors $\vec{P}(t) = \langle\chi(t)|\ \vec{\sigma}\ |\chi(t)\rangle$ with the spinor state $|\chi\rangle = \cos(\vartheta/2)|\uparrow\rangle + e^{i\varphi}\sin(\vartheta/2)|\downarrow\rangle$ in the z-eigenbasis. The coloured lines mark the evolution paths carried out in the experiment of section 4.3 in the laboratory frame of reference in the case of $n = 1$ in (10) with the frequencies specified in the legend. The evolution paths follow the description of (4). The initial polarisation vectors are all oriented in y-direction and the initial magnetic field is oriented in x-direction. Initially, all polarisation vectors are changed towards the same direction. With time, the field directions and the resulting spin manipulations diverge for different rotation frequencies. The higher the frequency, the smaller become the distance covered on the unit sphere and the solid angle enclosed by the evolution paths.

3. Design of the rotating field generator

3.1. Previous rotating field generators

A rotating field generator without material in the beam path was already used successfully in a polarimeter experiment before with a voluminous geometry of two perpendicular split pair coils [7]. A long solenoid was implemented on each side of a beam free of material. In the gap in between, the magnetic field is homogeneous like in the gap of an iron yoke. Demirel *et al* then used an alternative approach for a device for polarimetry with material in the beam. For the interferometer experiment, a miniaturisation of the coil used by Demirel *et al* was realised. The interferograms had low contrast ~10% because unintended phases were induced by the material in the beam. The implementation of the necessary water cooler was also complex.

3.2. Conditions

The requirements on the rotating field generator for an interferometric experiment are:

(i) smaller diameters than the rotating field generator of Demirel *et al* for a polarimeter,

(ii) no material in the beam cross-section to avoid dephasing,

(iii) possible adjustment of the field towards an arbitrary direction perpendicular to the neutron beam to make a rotating field possible,

(iv) a possible water cooling system for the coil, and

(v) a sudden field transition to induce Larmor precession.

The requirment (iv) is necessary to minimise the thermal disturbance around the coil which can degrade the neutron optical effect of the interferometer crystal.

The Mashhoon phase is proportional to the rotation frequency and the time of interaction. As more complex cyclic evolution paths are necessary for higher values of n, the case of $n = 1$ is considered from now on. In this case, the maximum angular velocity $f_{\max}$ for cyclic evolution paths of the polarisation vector is limited dependent on the interaction time T via $f_{\max}\,\mathrm{T} = \text{const}$. With an increased length of the coil and therefore interaction time, the maximum phase shift stays constant while the field homogeneity inside the coil is generally increased and the maximum frequency is conveniently reduced. Neutron interferometers of scew-symmetric design as in figure 1 provide more room than usual triple Laue interferometers for manipulators in single arms of an interferometer. The maximum length of 57.7 mm between two crystal plates of the available scew-symmetric interferometer limits the space for the water cooling housing. In practice, the coil mounter inside the water cooler is constrained to a longitudinal diameter Δy of 50 mm. Due to the dimensions of the interferometer, the dimensions of the coil Δx and Δz must also be short.

Empirically, at the instrument S18 at the High-Flux reactor in Grenoble, France, a good trade-off between the count rate and the contrast of interferograms is achieved with an aperture of 5 mm × 5 mm in front of the interferometer. As each plate of the interferometer horizontally widens the beam by the plate diameter of 3 mm, the rotating field generator is placed where the beam cross-section is smallest. The inhomogeneities of the field

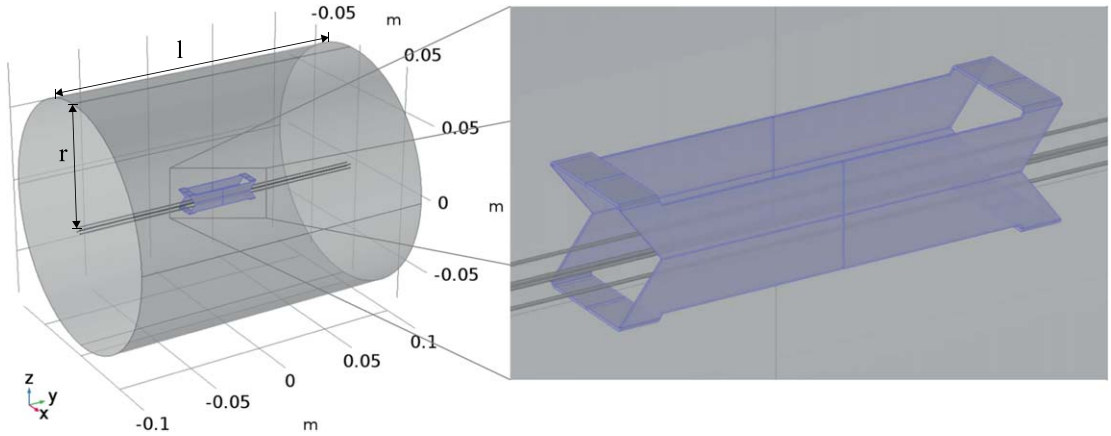


Figure 3. The simulated geometry of the conducting material of one winding (blue) of the rotating field generator in the volume (grey) in which the fields were simulated. Depicted to the right is a magnification of the rotating field generator. The four lines through the coil are along paths parallel to the centre axis. They were used to calculate the magnetic fields on them depicted in figure 5.

over the beam cross-section are thereby reduced. This is the case in path I of the interferometer in front of the respective reflecting plate (see figure 1) where the beam cross-section is 8 mm $\times$ 5 mm. On this cross-section, the coil must not have material and the homogeneity of the magnetic field must be high. To avoid depolarisation, a magnetic guide field will be applied in the interferometer region, which is not depicted in the experimental concept of figure 1. The guide field must be locally compensated inside the rotating field generator. For a 2π Larmor precession in the static case of $\Omega = 0$ and with $\vec{B} \perp \vec{S}$, the condition $|B_0 \Delta y| \approx 500$ G mm must be fulfilled which is equivalent to a field strength of 10 G on the estimated length of 50 mm. This field amplitude must be obtained for a reasonable current ~1 A. The necessary field amplitudes for cyclic evolutions with higher frequencies are achieved with lower currents (see (11)). To generate the rotating magnetic field, two independently operable windings with fields perpendicular to each other and to the beam must be implemented. In addition, corresponding to the magnetic field of (5), sinusoidal currents with a phase shift of 90° must be employed.

3.3. Field simulations

As the most easily realised geometry with a free beam path, a pair of coils in modified Helmholtz geometry above and below the beam was simulated first. It can be considered as a kind of split pair coil in the limit of each solenoids heigth reduced to a minimum. The geometry finally used as rotating field generator is shown in figure 3. Its winding is similar to a static spin rotator stretched in longitudinal length. The only difference are the free windows for the neutron beam where the coil is wound above and below the beam like in a Helmholtz coil (compare the fabricated coil in figure 6(b)).

Different geometries of windings were designed and their fields simulated with a finite element analysis software. Because both perpendicular windings have the same geometry, any superposition of their fields can be equivalently described as generated with one winding with an according orientation. Thus, simulating both windings is not necessary. In the centre of the winding, the field is oriented with a symmetry axis of the winding we define as z-axis. The beam direction was already set as y-axis. The remaining x-axis is chosen to compose a right-handed system with the other axes. To obtain the qualitative field characteristics, each winding was assumed to be composed of a reasonable number of turns with a current of 1 A. For a good approximation of the magnetic fields, also the boundary conditions were considered. The boundary surfaces $\mathcal{S}$ of the volume wherein the simulation takes place are assumed to be magnetic insulators which force the relation $0 = \vec{n}(\vec{r}) \cdot \vec{B}(\vec{r})$ with normal vector to some boundary surface $\vec{n}(\vec{r})$ to uphold for all position vectors $\vec{r} \in \mathcal{S}$. With the distinguished direction of the beam, the simulation volume is chosen cylindrically. Therefore, the fields in the vicinity of the coil, positioned in the centre of the volume, are influenced by the longitudinal length l and the radius r of the cylinder and converge with increasing dimensions. The simulation volume was fixed when increases in diameters only marginally changed the results of the fields in the coil at $l = 200$ mm and $r = 80$ mm (see figure 3 again). At this point, convergence was reached in terms of these qualitative purposes.

The simulated field of the modified Helmholtz coil has pronounced inhomogeneities in field direction and amplitude over the beam cross-section (not shown). The minimised heigth of the solenoids, necessary to reduce the diameters for an interferometer experiment, reduces the field homogeneity. The field transition on the centre axis is about 20 mm long. In the installation process in a polarimeter, the modified Helmholtz coil could not be aligned properly with the guide field and its test was unsuccessful.

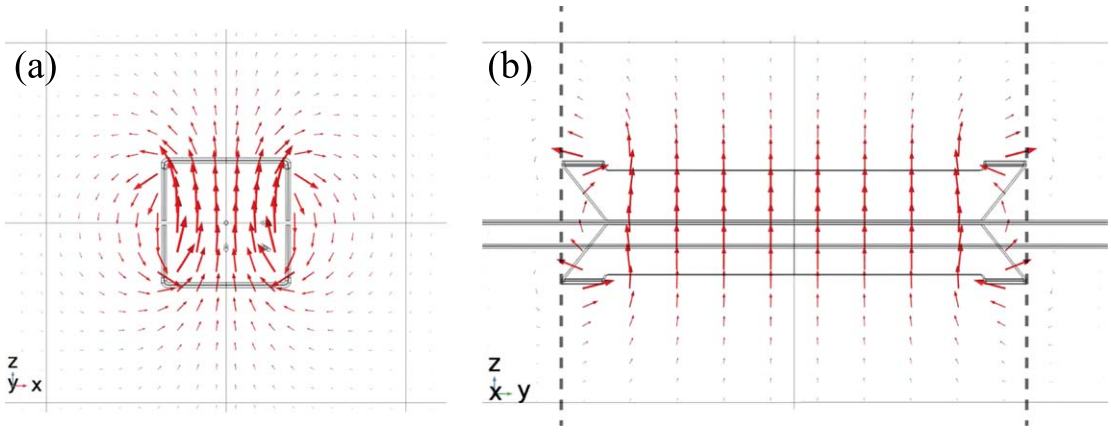


Figure 4. The simulated magnetic field in the (a) centre $x-z$-plane and (b) centre $y-z$-plane of the coil. The dashed lines mark the beginning and the end of the winding.

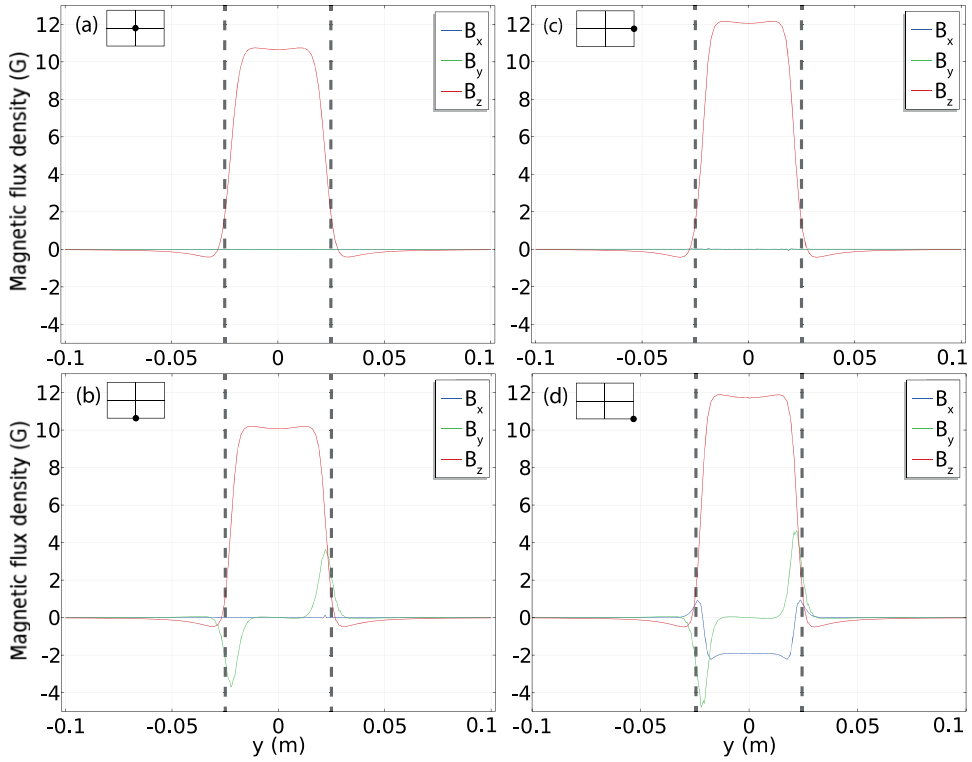


Figure 5. The simulated magnetic field strengths on different paths on the beam cross-section parallel to the centre axis of the coil specified graphically besides the lettering (compare figure 3). Transitions on the (a) centre, (b) lower, (c) right, and (d) lower right paths of the expected neutron beam. The dashed lines mark the beginning and the end of the winding as in figure 4(b).

The simulated magnetic field of the rotating field generator in the centre x-z-plane is depicted in figure 4(a) and the simulated field in the centre $y-z$-plane is depicted in figure 4(b). Both fields are homogeneous in field direction and magnitude near the centre and more diverged close to the winding. The field along the centre axis, presented in figure 5(a), is purely oriented in z-direction with a maximum amplitude of more than 10.5 G which is of the order of the amplitude specified as necessary for spin manipulations of 10 G. In front and behind the coil, an opposing field of 0.5 G emerges. The transition length, defined as distance between minimum and maximum, can be estimated to about 20 mm. For a first assessment of the suddenness caused by this field transition length, the length must be compared with the Larmor precession length of the order of 100 mm in typical guide field strengths and for the typically used thermal neutrons with $\lambda \sim 2$ Å. The simulated transition lengths are less than one order of magnitude shorter and therefore not sufficiently short for a sudden field transition. However, in fact it turned out that the field transition of the rotating field generator was sufficiently short for inducing the linear phase shift in the experiment expected from the calculation (see section 4.3). The

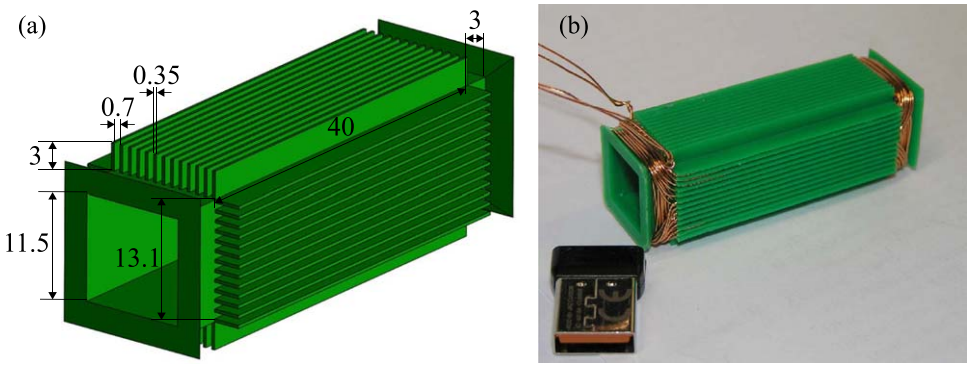


Figure 6. (a) Specific diameters of the coil mount in millimetres (mm) and (b) a photo of the coil wound on the mount with two separate windings with perpendicular orientation and an USB stick for comparision. The wires are at both ends wound around the window for the neutron beam. In between, the grooves hold the wires parallel to the beam.

difference to the inadequate coil with modified Helmholtz geometry does not lie in the adiabaticity but in the field homogeneity. This is a consequence of the wires on different heights relative to the beam which cancel out each other's magnetic flux in x-direction and result in a flux tube with z-orientation.

On beam paths other than the centre axis, other field directions are present. For the three extreme lower, right and lower right transitions of the beam at positions $(x,\ z) \in \{(0\ \text{mm}, -2.5\ \text{mm}), (4\ \text{mm}, 0\ \text{mm}), (4\ \text{mm}, -2.5\ \text{mm})\}$ shifted to the centre axis, the fields are presented in figures 5(b)–(d). On these beam paths the largest magnetic field deviations from the centre beam path are present. Due to symmetry, the fields on the presented four beam paths suffice to assess the field homogeneity over the whole beam cross-section. At the middle lower point (b) of the beam, a field in y-direction with a maximum amplitude of 3.5 G occurs at the transitions. The z-field is slightly reduced. At the middle right point (c), the z-field deviates from the field in the centre by a 10% increase of maximum field strength. At the corner point (d), y-fields of 4.5 G occur at both transitions with opposing signs and an x-field around 2 G is present inside the coil. The respective opposing field outside the coil is 1 G. If we consider small or cyclic spin manipulations inside the rotating field generator, the opposing y-fields at the transitions cancel each other to first order. The constant x-field has the same sign on diagonals of the cross-section only and cannot be used to homogeneously strengthen the perpendicular field of the other winding. As this most problematic constant x-field occurs at the diagonals, a circular/elliptical aperture could increase the field homogeneity. However, no serious problems with the rectangular aperture occured in the experimental tests.

3.4. Fabrication

The coil mount (see figure 6(a) for exact dimensions) was constructed and 3D-printed. With a length of approximately 50 mm, the coil is short enough to fit in various silicon perfect crystal interferometers [34]. Two solenoids with perpendicular orientations are wound on the mount with 24 turns in two layers each (see figure 6(b)). Their fields can be superposed to an arbitrary direction perpendicular to the beam. The wires are at both ends wound around the window. In between, grooves hold the wires parallel to the beam. A water cooling system for application in neutron interferometry was constructed where the entire coil is put in a water filled box. The beam can pass the coil without interacting with any water or material of the coil.

4. Performance test in a neutron polarimeter experiment

4.1. Set-up

The polarimeter experiment was carried out at the TRIGA Mark II reactor of the TU Wien, Vienna, with a thermal power of 250 kW. A graphite monochromator selects neutrons with a wavelength of 1.7 Å. The downstream set-up is depicted in figure 7. Two CoTi multilayer supermirror arrays, from now on called *supermirrors*, are used as polariser and analyser. Out of an unpolarised beam, each supermirror produces a neutron beam with an approximate degree of polarisation of 92%. Both polariser and analyser are oriented in z-direction which is therefore the quantisation axis. This is the basis of all considerations regarding our coordinate system. Between the supermirrors, a guide field in z-direction is produced with a pair of coils in modified Helmholtz geometry. A ^{3}He counter tube detects the neutrons reflected by the analyser. In the guide field, two direct current auxiliary coils (DC1 and DC2) and the rotating field generator are installed. An aperture in front of the rotating field generator trims the neutron beam to the cross-section of 5 mm $\times$ 8 mm which we plan to use

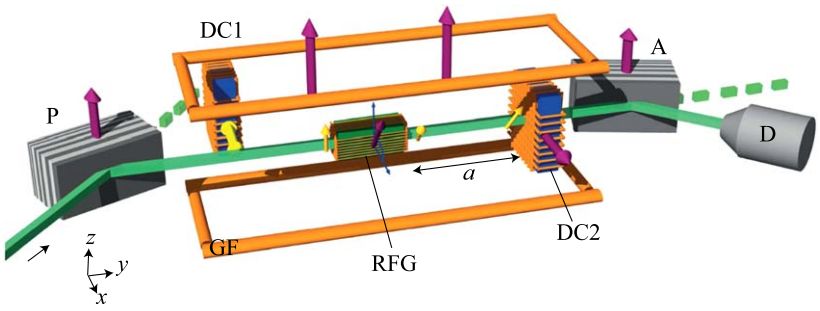


Figure 7. The set-up of the final measurements downstream the monochromator: incoming neutron beam, polariser (P), analyser (A), the detector (D), the coils of the guide field (GF) in modified Helmholtz configuration, the direct current auxiliary coils (DC1 and DC2), the rotating field generator (RFG). Effective local magnetic fields and the orientation of the polarisation vector at specific positions are pictured as purple and orange arrows respectively. Neutrons with a wavelength of 1.7 Å propagate to the polarising supermirror. It reflects only neutrons with up-spin state which enter the region of the guide field. Neutrons with down-spins are transmitted by the supermirrors (dashed beams) and absorbed. DC1 is removed in this final step and only used for the adjustment procedure. The neutrons interact with the rotating field of the rotating field generator and the static field of DC2. The distance a between rotating field generator and DC2 produces a $\left(2+\frac{1}{2}\right)\pi$ Larmor precession between them. Those neutrons with up-spins at the analysing supermirror are reflected towards the detector.

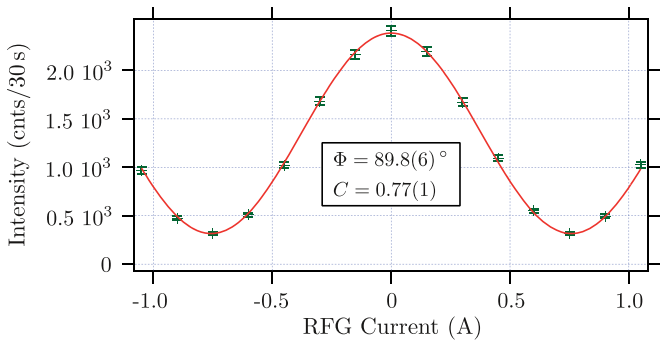


Figure 8. Intensity dependent on the current for the x-field and a respective rotation of the spin orientation in the rotating field generator in the static case $\Omega = 0$ while the guide field of 9 G is compensated. The most important fit parameters of the sinusoidal fit (red graph) are stated in the text box.

in the coming neutron interferometer experiment. In this set-up, DC1 determines the spin orientation which enters the rotating field generator while DC2 determines the analysed spin orientation.

4.2. Stationary field

In the experimental procedures described in this section, all spin manipulations, specifically with the rotating field generator, are generated with static fields ($\Omega = 0$). All three coils have two independent windings which generate fields in x and z-direction. For spin manipulations with either of them, the guide field is locally compensated with the z-coil and an effective x-field is implemented. Scanning the current for the x-field produces intensity modulations henceforth called *polarograms* which represent the change of the polarisation vector. First, only a single coil inside the guide field is in operation at a time. A polarogram produced by scanning the x-field of the rotating field generator is depicted in figure 8. It is symmetric with a maximum count rate of more than 2000 neutrons per 30 s which is sufficiently high to guarantee the qualtity of the measurements. For sinusoidal intensity changes dependent on the x-current I_x, a fit function $g(I_x) = A_0 + A\sin(\omega_{\text{fit}} I_x + \Phi)$ was chosen, with offset A_0, amplitude A, the angular velocity of the fit function ω_{fit}, and the phase Φ. The current for the π-flip of the polarisation vector is about 750 mA. The depicted polarogram has a maximum contrast $C = 77\%$ inside a guide field of 9 G while the contrast is reduced with other guide field strengths. The guide field was fixed at 9 G for all successive measurements. In this guide field, the polarograms of either auxiliary coil have a contrast of about 86%.

From here on, multiple coils are operated in combination in the guide field. To get an estimation of the effective length of the rotating field generator, DC1 and DC2 are positioned with a distance of a 4π Larmor precession between them. Inducing a rotation by $\pi/2$ with DC1 and scanning the x-current of DC2, the polarograms have a contrast of 79%. When positioning the rotating field generator in between with a distance of

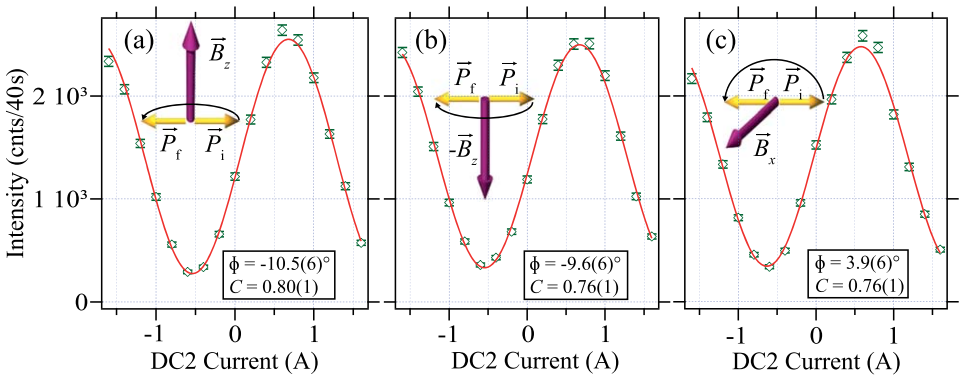


Figure 9. Polarograms recorded by rotating the polarisation vector by $\pi/2$ with DC1, a π rotation induced by different static fields of the rotating field generator and scanning the x-current of DC2. The static fields of the rotating field generator are (a) a $+z$-field parallel to the guide field, (b) a $-z$-field antiparallel to the guide field, and (c) an x-field. Each field rotates the same initial polarisation vector $\vec{P}_\mathrm{i}$ into the same final polarisation vector $\vec{P}_\mathrm{f}$. The most important fit results are stated in the text boxes.

a 2π Larmor precession to DC1, DC2 is displaced 40 mm to adjust the distance to a 2π Larmor precession between it and the rotating field generator. This effective length of the rotating field generator $l_\mathrm{eff}^\mathrm{meas}$ is important to assess the time of interaction with the field of the rotating field generator. The absolute error is estimated as 1 mm which is equivalent to a relative error of 2.5%. With the described distances and rotation angles of $\pi/2$ with DC1 and π with static fields of the rotating field generator, polarograms were recorded by scanning the x-current of DC2 (see figure 9). The π-flip of the rotating field generator was induced with three different orientations of the static field, namely a $+z$-field parallel to the guide field, a $-z$-field antiparallel to the guide field, and an x-field. The maximum contrast of 80% is reached with the $+z$-field, while both $-z$ and x-field result in a contrast of 76%. The field changes at the transitions to the amplified guide field are minimal compared to the changes of field directions for $-z$ and x-field which results in a higher efficiency of the spin manipulation and a higher contrast when applying a $+z$-field.

4.3. Rotating field

From here on, the rotating field generator is supplied with alternating currents which have the same amplitude and are phase shifted by 90°. As the maximum frequency for cyclic evolutions, according to (11), calculates to $f_\mathrm{max} \sim 58$ kHz in the case $n = 1$ and with the estimated length of the coil of 40 mm, frequencies from 0 kHz to 40 kHz were used. Higher frequencies with their reduced spin rotations (see figure 2) make the following adjustments more difficult: to realise the cyclic paths for a fixed rotation frequency, a $+y$-polarisation vector is prepared by DC1 and then propagates further to the rotating field generator. DC2 rotates the polarisation vector by $\pi/2$ around the x-axis. With this combination of spin manipulations, the intensity is minimum. Generating a rotating magnetic field inside the rotating field generator, the same minimum intensity is produced with a specific amplitude for each frequency of the rotating field (see (11)). A rotating magnetic field with this amplitude realises a cyclic spin evolution depicted in figure 2. In this case, the spin states entering and leaving the rotating field generator can only differ in their phases. With the adjustment of the amplitude, the cyclic spin evolution of $|\pm y\rangle$-eigenstates are similar but inversions through the origin. Fixing the non-zero field amplitude for the minimum of the count rates and recording polarograms by scanning the x-current of DC2 produced similar contrasts ~75% for each frequency from 10 kHz to 40 kHz.

By removing DC1 from the polarimetric set-up, as depicted in figure 7, a $+z$-polarisation vector is produced as input for the rotating field generator. The corresponding spin state $|+z\rangle$ can be written as equally weighted superposition of $|\pm y\rangle$-eigenstates. A relative phase gained inside the rotating field generator between the eigenstates $|\pm y\rangle$ rotates the resulting polarisation vector in the $x-z$-plane (see (14)). When DC2 is displaced to a position of a $(2 \pm \frac{1}{2})\pi$ Larmor precession from the rotating field generator, the polarisation vector of the input for DC2 lies in the $y-z$-plane and is rotated dependent on the value of the induced relative phase. Scanning the x-current of DC2, the phase information is accessible via polarograms. For higher statistical confidence, ten polarograms were recorded for each rotation frequency. Typical examples for each frequency with different phases are presented in figures 10(a)–(e). The average contrasts for each frequency are plotted in figure 10(f). Although there seems to be a systematic oscillation of the contrast in the final measurements (figure 10(f)), the distance of DC2 is adjusted accurately. If DC2 was misplaced, the contrast would oscillate with a maximum at the flip frequency with a phase shift of 180° at about 25 kHz (compare final results of figure 11). The required non-adiabatic field transition is more difficult to establish with a rotating field. In the static case, only the field

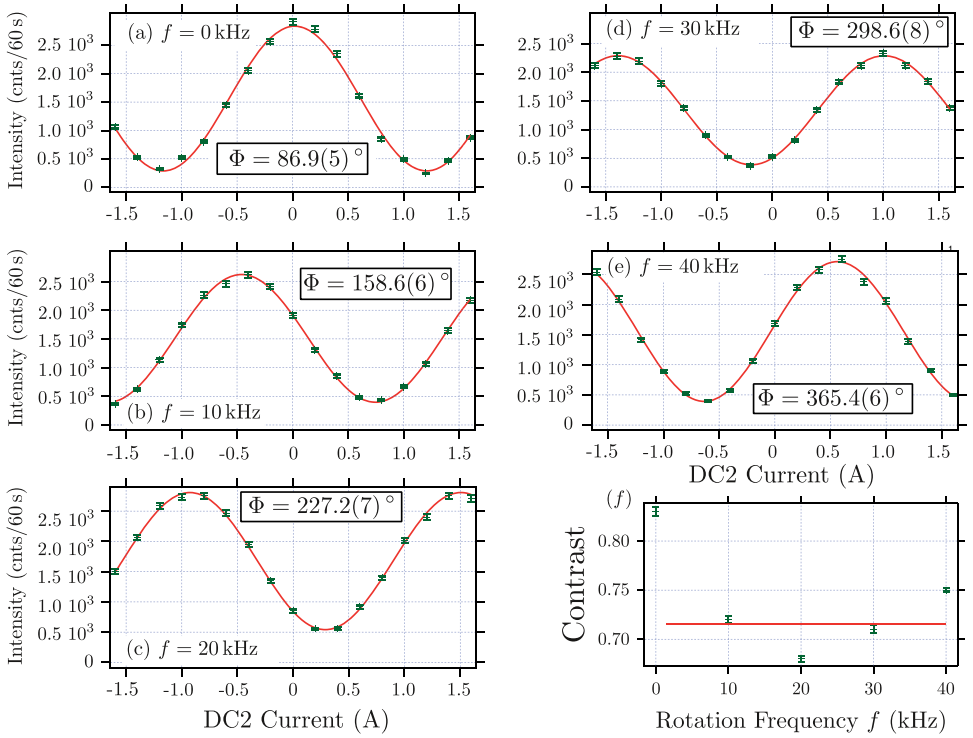


Figure 10. (a)–(e) Polarograms observed for rotation frequencies ranging from 0 kHz to 40 kHz. The phases, stated in the text boxes, increase with higher frequency. (f) Average contrast of the set of ten polarograms dependent on the rotation frequency.

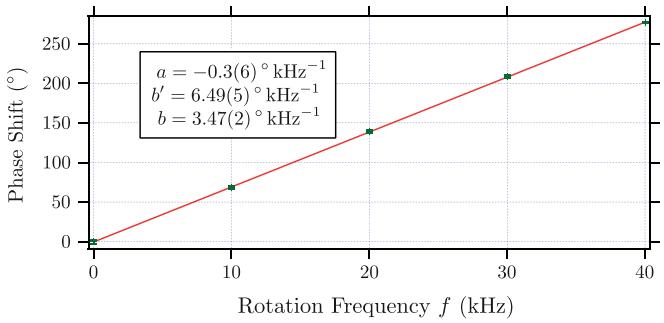


Figure 11. The average phase shifts of polarograms dependent on the frequency with linear regression model of (15) and corresponding fit results.

strength is changed at the transitions while for genuine rotations also the field direction is constantly changing during the transitions. Therefore, a constant was fitted to the contrasts from 10 kHz to 40 kHz in figure 10(f).

The average phase of the polarograms recorded with the static field $\Omega = 0$ was used as a reference for the induced phase shift. Finally, the average phases relative to this reference are plotted in figure 11. As a linear phase shift is expected from (12), a linear fit model dependent on the frequency f of the form

$$\Delta\phi_{\mathrm{Mh}}(f) = a + b'f \tag{15}$$

was applied. The resulting fit parameters are

$$a = -0.3(6)^\circ, \text{ and } b' = 6.94(5)^\circ\,\mathrm{kHz}^{-1}. \tag{16}$$

The result for a is in accordance with the reference of the average phase for $\Omega = 0$. The slope b' is the phase difference between y-eigenstates. For an estimation of the slope b of the phase gained by a single y-eigenstate, the slope b' is divided by 2 to

$$b = 3.47(2)^\circ\,\mathrm{kHz}^{-1}. \tag{17}$$

For neutrons with a wavelength of 1.7 Å, this value is theoretically achieved with an effective field length $l_{\mathrm{eff}}^{\mathrm{theo}} = 45$ mm, a difference to the measured value of $l_{\mathrm{eff}}^{\mathrm{meas}} = 40$ mm five times the estimated error of 1 mm.

5. Discussion

The effective length of the coil can be measured via two different approaches: the displacement of DC2 from section 4.2 and the slope of the linear fit to the phase. While the former relies on a difference in the Larmor precession, the latter relies on the induced phase shifts. Regarding the Larmor precession, when compensating the guide field in the rotating field generator, a small but finite field on the outside of the coil strengthens the guide field and reduces the distance for a 2π Larmor precession. By this mechanism, the effective length of the coil is underestimated. On the other hand, at the field transitions of the rotating field generator only an insignificant field is present where both Larmor precession as well as spin-rotation coupling are negligable. This is a mechanism by which the displacement of DC2 is longer than the diameter where spin-rotation coupling is induced.

The magnetic properties of the coil could also be used for other neutron interferometer experiments. The present design was not quantitatively optimised. However, possible improvements at the required conditions are expected to be marginal while generating more complex geometries of the coil mount. The field homogeneity could be increased by relatively reducing the beam cross-section compared to the coil in transversal direction in cases of less tight restrictions on this diameters or if less count rate is acceptable. Another option is to use a circular/ellipsoidal aperture. Further reductions of the longitudinal diameter are expected to oppress the non-adiabatic property of the field transition. Moreover, the coil geometry can be modified for any other application sensitive to material with similarly strong conditions on the magnetic field and the diameters.

6. Conclusion

A rotating field generator is designed for an interferometer experiment. Its magnetic field is simulated, an according coil mount as well as a water cooler are fabricated and the device is successfully tested in a polarimeter experiment. The field simulations show a sufficient field homogeneity. Although the field transition is initially indicated as too long, the experimental results accord qualitatively with the assumption of a sudden field transition. The presented rotating field generator is suited for the proposed experiment by Mashhoon *et al* [4] investigating spin-rotation coupling in neutron interferometry.

Acknowledgments

This work was financed by the Austrian Science Fund (FWF), Project No. P 30677-N20.

ORCID iDs

Armin Danner https://orcid.org/0000-0003-3244-010X
Stephan Sponar https://orcid.org/0000-0002-6568-6045
Yuji Hasegawa https://orcid.org/0000-0001-5175-0408

References

[1] Sagnac G 1913 Sur la preuve de la réalité de l'éther lumineux par l'expérience de l'interférographe tournant *Comptes Rendus Acad. Sci.* **157** 1410–1413
[2] Mashhoon B 1988 Neutron interferometry in a rotating frame of reference *Phys. Rev. Lett.* **61** 2639–42
[3] Mashhoon B, Neutze R, Hannam M and Stedman G E 1998 Observable frequency shifts via spin-rotation coupling *Phys. Lett.* A **249** 161–6
[4] Mashhoon B and Kaiser H 2006 Inertia of intrinsic spin *Physica* B **385** 1381–3
[5] Demirel B, Sponar S and Hasegawa Y 2015 Measurement of the spin-rotation coupling in neutron polarimetry *New J. Phys.* **17** 023065
[6] Ramsey N F 1950 A molecular beam resonance method with separated oscillating fields *Phys. Rev.* **78** 695–9
[7] Weinfurter H and Badurek G 1990 Measurement of Berry's phase for noncyclic evolution *Phys. Rev. Lett.* **64** 1318–21
[8] Badurek G, Weinfurter H, Gähler R, Kollmar A, Wehinger S and Zeilinger A 1993 Nondispersive phase of the Aharonov-Bohm effect *Phys. Rev. Lett.* **71** 307–11
[9] Hasegawa Y, Menhart S, Meixner R and Badurek G 1997 Noncommutation of Pauli spin operators in neutron polarimetry *Phys. Lett.* A **234** 322–8
[10] Wagh A G, Badurek G, Rakhecha V C, Buchelt R J and Schricker A 2000 Neutron polarimetric separation of geometric and dynamical phases *Phys. Lett.* A **268** 209–16
[11] Rauch H, Treimer W and Bonse U 1974 Test of a single crystal neutron interferometer *Phys. Lett.* A **47** 369–71
[12] Summhammer J, Badurek G, Rauch H, Kischko U and Zeilinger A 1983 Direct observation of fermion spin superposition by neutron interferometry *Phys. Rev.* A **27** 2523–32
[13] Wagh A G, Rakhecha V C, Summhammer J, Badurek G, Weinfurter H, Allman B E, Kaiser H, Hamacher K, Jacobson D L and Werner S A 1997 Experimental separation of geometric and dynamical phases using neutron interferometry *Phys. Rev. Lett.* **78** 755–9

[14] Hasegawa Y, Loidl R, Badurek G, Baron M and Rauch H 2003 Violation of a Bell-like inequality in single-neutron interferometry *Nature* **425** 45–8
[15] Hasegawa Y, Loidl R, Badurek G, Baron M, Manini N, Pistolesi F and Rauch H 2002 Observation of off-diagonal geometric phases in polarized-neutron-interferometer experiments *Phys. Rev.* A **65** 052111
[16] Klepp J, Sponar S and Hasegawa Y 2014 Fundamental phenomena of quantum mechanics explored with neutron interferometers *Progr. Theor. Exp. Phys.* **2014** 082A01
[17] Badurek G, Rauch H and Summhammer J 1983 Time-dependent superposition of spinors *Phys. Rev. Lett.* **51** 1015–8
[18] Golub R, Gähler R and Keller T 1994 A plane wave approach to particle beam magnetic resonance *Am. J. Phys.* **62** 779–88
[19] Golub R and Gähler R 1987 A neutron resonance spin echo spectrometer for quasi-elastic and inelastic scattering *Phys. Lett.* A **123** 43–8
[20] Grigoriev S V, Kraan W H and Rekveldt M T 2004 Four-wave neutron-resonance spin echo *Phys. Rev.* A **69** 043615
[21] Sponar S, Klepp J, Loidl R, Filipp S, Badurek G, Hasegawa Y and Rauch H 2008 Coherent energy manipulation in single-neutron interferometry *Phys. Rev.* A **78** 061604
[22] Bleser E J *et al* 1985 Superconducting magnets for the CBA project *Nucl. Instrum. Methods Phys. Res.* A **235** 435–63
[23] Amemiya N, Sogabe Y, Sakashita M, Iwata Y, Noda K, Ogitsu T, Ishii Y and Kurusu T 2016 Magnetisation and field quality of a cosine-theta dipole magnet wound with coated conductors for rotating gantry for hadron cancer therapy *Supercond. Sci. Technol.* **29** 024006
[24] Berry M V 1984 Quantal phase factors accompanying adiabatic changes *Proc. Royal Soc. Lond.* A **392** 45–57
[25] Berry M V 1987 Quantum phase corrections from adiabatic iteration *Proc. Royal Soc. Lond.* A **414** 31–46
[26] Aharonov Y and Anandan J 1987 Phase change during a cyclic quantum evolution *Phys. Rev. Lett.* **58** 1593–6
[27] Bitter T and Dubbers D 1987 Manifestation of Berry's topological phase in neutron spin rotation *Phys. Rev. Lett.* **59** 251–4
[28] Richardson D J, Kilvington A I, Green K and Lamoreaux S K 1988 Demonstration of Berry's Phase Using Stored Ultracold Neutrons *Phys. Rev. Lett.* **61** 2030–3
[29] Hasegawa Y and Badurek G 1999 Noncommuting spinor rotation due to balanced geometrical and dynamical phases *Phys. Rev.* A **59** 4614–22
[30] Durstberger K 2002 Geometric phases in quantum theory *Master Thesis* TU Wien
[31] Hehl F W and Ni W-T 1990 Inertial effects of a Dirac particle *Phys. Rev.* D **42** 2045–8
[32] Ryder L 1998 Relativistic treatment of inertial spin effects *J. Phys.* A **31** 2465
[33] Badurek G 1982 Physik polarisierter Neutronen *Habilitationsschrift* (German)TU Wien
[34] Rauch H and Werner S A 2015 *Neutron Interferometry* (Oxford: Oxford University Press)